Autophagy

Taylor & Francis
Taylor & Francis Group

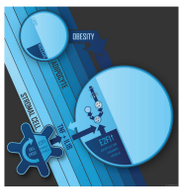

Autophagy

ISSN: 1554-8627 (Print) 1554-8635 (Online) Journal homepage: http://www.tandfonline.com/loi/kaup20

Alterations of autophagy in the peripheral neuropathy Charcot-Marie-Tooth type 2B

David Colecchia, Mariangela Stasi, Margherita Leonardi, Fiore Manganelli, Maria Nolano, Bianca Maria Veneziani, Lucio Santoro, Eeva-Liisa Eskelinen, Mario Chiariello & Cecilia Bucci

To cite this article: David Colecchia, Mariangela Stasi, Margherita Leonardi, Fiore Manganelli, Maria Nolano, Bianca Maria Veneziani, Lucio Santoro, Eeva-Liisa Eskelinen, Mario Chiariello & Cecilia Bucci (2017): Alterations of autophagy in the peripheral neuropathy Charcot-Marie-Tooth type 2B, Autophagy, DOI: 10.1080/15548627.2017.1388475

To link to this article: https://doi.org/10.1080/15548627.2017.1388475

Accepted author version posted online: 13 Nov 2017.

Alterations of autophagy in the peripheral neuropathy Charcot-Marie-Tooth type 2B

David Colecchia[1], Mariangela Stasi[2], Margherita Leonardi[1], Fiore Manganelli[3], Maria Nolano[4], Bianca Maria Veneziani[5], Lucio Santoro[3], Eeva-Liisa Eskelinen[6], Mario Chiariello[1,*], and Cecilia Bucci[2,*]

[1]Consiglio Nazionale delle Ricerche, Istituto di Fisiologia Clinica and Istituto Toscano Tumori-Core Research Laboratory, Signal Transduction Unit, AOU Senese, Siena, Italy

[2]Department of Biological and Environmental Sciences and Technologies (DiSTeBA), University of Salento, Lecce, Italy

[3]Department of Neurosciences, University of Naples "Federico II", Napoli, Italy

[4]Salvatore Maugeri Foundation, Institute of Telese Terme (BN), Italy

[5]Department of Molecular Medicine and Medical Biotechnologies, University of Naples "Federico II", Naples, Italy

[6]Department of Biosciences, Division of Biochemistry and Biotechnology, University of Helsinki, Finland

*Corresponding authors: Cecilia Bucci, Dipartimento di Scienze e Tecnologie Biologiche ed Ambientali, Università del Salento, Via Provinciale Monteroni 165, 73100 Lecce, Italy. Tel.: +39 0832 298900; Fax: +39 0832 298626; Email: cecilia.bucci@unisalento.it; Mario Chiariello, Consiglio Nazionale delle Ricerche, Istituto di Fisiologia Clinica and Istituto Toscano Tumori-Core Research Laboratory, Signal Transduction Unit, AOU Senese, Siena, Italy. Tel.: +39 0577 231274; Fax: +39 0577 280599; Email: mario.chiariello@cnr.it

Abstract

Charcot-Marie-Tooth type 2B (CMT2B) disease is a dominant axonal peripheral neuropathy caused by 5 mutations in the *RAB7A* gene, a ubiquitously expressed GTPase controlling late endocytic trafficking. In neurons, RAB7A also controls neuronal-specific processes such as NTF (neurotrophin) trafficking and signaling, neurite outgrowth and neuronal migration. Given the involvement of macroautophagy/autophagy in several neurodegenerative diseases and considering that RAB7A is fundamental for autophagosome maturation, we investigated whether CMT2B-causing mutants affect the ability of this gene to regulate autophagy. In HeLa cells, we observed a reduced localization of all CMT2B-causing RAB7A mutants on autophagic compartments. Furthermore, compared to expression of $RAB7A^{WT}$, expression of these mutants caused a reduced autophagic flux, similar to what happens in cells expressing the dominant negative $RAB7A^{T22N}$ mutant. Consistently, both basal and starvation-induced autophagy were strongly inhibited in skin fibroblasts from a CMT2B patient carrying the $RAB7A^{V162M}$ mutation, suggesting that alteration of the autophagic flux could be responsible for neurodegeneration.

Key words: autophagy, Charcot-Marie-Tooth disease, Charcot-Marie-Tooth type 2B, endocytosis peripheral neuropathy, RAB7, RAB7A.

Abbreviation list: BAF, bafilomycin A_1; CMT2B, Charcot-Marie-Tooth type 2B; FM, full medium; GABARAP, GABA type A receptor-associated protein; GDP, guanosine diphosphate; GTP, guanosine triphosphate; MAP1LC3B/LC3B, microtubule associated protein 1 light chain 3 beta; MAPK1, mitogen-activated protein kinase 1; RAB7A, RAB7A, member RAS oncogene family; SQSTM1/p62, sequestosome 1; TUBA1A, tubulin alpha 1a; WT, wild type.

Introduction

More than 80 genes have been involved in Charcot-Marie-Tooth (CMT), a rare inherited peripheral neuropathy, and several of them are involved in the regulation of intracellular vesicular trafficking.[1,2] The CMT type 2B (CMT2B) is a dominant axonal form caused by 5 mutations (L129F, K157N, N161T, V162M and the recently identified N161I) in the *RAB7A* gene,[3-6] and it is characterized by prominent sensory loss, lower legs muscle atrophy, high frequency of foot ulcers and recurrent infections leading to toe amputations.[7-9]

RAB7A, hereafter referred to as RAB7, is a ubiquitous small GTPase regulating late endocytic transport.[10-12] To investigate the role of RAB7 in the endocytic pathway, previous studies have used the dominant negative $RAB7^{T22N}$ mutant, which displays reduced affinity for GTP and impaired nucleotide exchange, thus being mainly GDP-bound, and the constitutively active $RAB7^{Q67L}$ mutant, which displays impaired intrinsic GTP hydrolysis, thus being mainly GTP-bound.[13]

Others and we have demonstrated that CMT2B-causing RAB7 mutants show higher nucleotide K_{off}, thus releasing nucleotides faster than expected and, consequently, displaying inhibited GTPase activity per binding event.[14-16] Indeed, given the higher K_{off} for GDP compared to the wild-type protein and the higher concentration of GTP compared to GDP in cells, CMT2B mutant proteins are mostly in the GTP-bound form and, thus, were initially predicted to be active mutants.[14] However, given that K_{off} for GTP is also increased compared to $RAB7^{WT}$,[14-16] thus determining early release of GTP, and that binding of GTP is not correctly regulated,[16] these mutants although being mainly GTP-bound and interacting more strongly with a number of

effector proteins,[14,16] could also display reduced efficiency in the activation of downstream specific effectors and pathways. In fact, studies on disease animal models established that in *Drosophila*, the presence of CMT2B mutant proteins induces sensory defects and dosage-dependent neurodegeneration due to partial loss of function,[17,18] while in zebrafish axon growth and guidance defects are due to gain-of-function mechanisms.[19] Therefore, depending on the kinetic requirements of the processes controlled by RAB7, these mutants could behave as inhibitory or active.

RAB7 controls specific neuronal functions such as NTF (neurotrophin) trafficking and signaling and it is responsible for retrograde axonal traffic, neurite outgrowth and neuronal migration,[20-24] besides interacting with and regulating assembly of 2 intermediate filament proteins, VIM (vimentin) and PRPH (peripherin), which are involved in neurite outgrowth and axonal regeneration.[25-31] Neuronal functions are highly dependent on protein synthesis and degradation, and a constitutive autophagic flux is fundamental for a number of key neuronal processes.[32-34] Perturbation of the autophagic flux indeed causes neurodevelopmental and neurodegenerative diseases and has been observed, for instance, in Alzheimer disease, Parkinson disease and amyotrophic lateral sclerosis.[33,34] Notably, RAB7 regulates autophagosomal maturation controlling the final step of maturation of late autophagic vesicles into autolysosomes, presumably involving fusion with lysosomes.[12,35-37]

In this manuscript we investigated the role of CMT2B-causing RAB7 mutant proteins in autophagy, demonstrating that expression of these mutants alters both basal and starvation-induced autophagy in HeLa cells. Furthermore, these finding were confirmed in patient skin

fibroblasts carrying the RAB7^{V162M} mutation suggesting that neurodegeneration could be due to altered autophagy.

Results

To investigate the role of CMT2B-causing RAB7 mutant proteins (RAB7^{L129F}, RAB7^{K157N,} RAB7^{N161T} and RAB7^{V162M}) on autophagy, we analyzed, by immunofluorescence analysis, colocalization of wild type and mutant proteins with the autopaghic vesicle marker LC3B. HeLa cells were analyzed after incubation in full medium to determine the basal level of RAB7 and LC3B colocalization, whereas starvation medium was used to induce the autophagic process, and bafilomycin A_1 (Baf), a drug inhibiting the vacuolar-type H^+-translocating ATPase (V-ATPase), was used to prevent the lysosomal turnover of the autophagosome content (**Fig. S1-S3**). Consistent with previous results,[35] RAB7^{WT} displayed a good colocalization rate with LC3B, which increased upon starvation (**Fig. 1A; Fig. S1-S3**). As expected, the constitutively active RAB7^{Q67L} mutant showed increased colocalization with LC3B both in full medium and in starvation medium (**Fig. 1A; Fig. S1-S2**). Interestingly, CMT2B-causing mutants showed a reduced colocalization rate in each of the conditions tested, comparable with that of the dominant negative RAB7^{T22N} mutant (**Fig. 1A; Fig. S1-S3**), indicating that CMT2B-causing mutants are less recruited to autophagic vesicles when compared with RAB7^{WT}. Based on the established role of RAB7 in autophagy,[35] the reduced localization of this protein on autophagic vesicles suggests potential functional consequences of RAB7 mutant expression on this process.

Autophagosome number is one of the main mechanistic factors through which the amplitude of autophagic activity is regulated.[38] Therefore, we analyzed the number of autophagosomes in cells expressing $RAB7^{WT}$ and mutant proteins. Interestingly, CMT2B-associated mutant proteins caused a reduction in the amount of autophagic vesicles in full medium, starvation medium and upon bafilomycin A_1 treatment, as compared to $RAB7^{WT}$ (**Fig. 1B**).

The analysis of the autophagic flux, obtained by the ratio between the amount of autophagic vesicles in basal conditions (FM) and upon protease inhibition (Baf),[39] showed a reduced autophagic flux upon expression of the CMT2B-causing RAB7 mutants and, as expected,[35] of $RAB7^{T22N}$, as compared to $RAB7^{WT}$ and $RAB7^{Q67L}$ proteins (**Fig. 1C**).

To confirm these data, we also used a different approach, immunoblot analysis, in order to monitor the abundance of LC3B-II on extracts of HeLa cells transfected with empty vector or expressing $RAB7^{WT}$ and mutant proteins and grown in full and starvation medium or treated with bafilomycin A_1. As shown in **Fig. 2A-C**, we again observed a reduced autophagic flux upon expression of CMT2B-causing mutants as compared to the wild-type protein, with all mutant proteins behaving similarly to the dominant negative T22N form of RAB7 in full medium and upon bafilomycin A_1 treatment. It is worth noting that effects obtained with the $RAB7^{T22N}$ mutant in immunofluorescence analysis are much stronger than the ones obtained by immunoblotting, as this mutant is generally less expressed and only with immunofluorescence can transfected cells be selected for analysis.

In order to further validate these data, we analyzed the autophagic flux also monitoring SQSTM1/p62 and GABARAP (**Fig. 2 D-F**), 2 additional well established autophagy markers.[39]

Data obtained using these markers confirmed that expression of the CMT2B-causing RAB7 mutant proteins reduced the autophagic flux compared to $RAB7^{WT}$. Interestingly, using these markers the expression of the constitutively active $RAB7^{Q67L}$ increased the autophagic flux, whereas expression of the dominant negative $RAB7^{T22N}$ caused a much stronger inhibition compared to the CMT2B-causing RAB7 mutant proteins, thus confirming the different nature of these mutants.

Altogether, these data strongly indicate that CMT2B-causing mutations negatively affect the role of RAB7 in the autophagic process.

In order to determine in which step the CMT2B-causing RAB7 mutant proteins inhibit autophagy, we used the tandem EGFP-mCherry-LC3B construct to monitor autophagic vesicle maturation (**Fig. 3**). The basis for the utility of EGFP-mCherry-LC3B as a reporter for autophagic flux lies in the higher sensitivity of EGFP fluorescence to the acidic environment of the autolysosome relative to mCherry. Indeed, cells with higher flux have lower green signal due to the fusion of autophagosomes with lysosomes, which increases the mCherry:EGFP ratio in the cell. Using ratiometric flow cytometry, it is possible to calculate the flux in each cell based on this ratio.[40] Taking advantage of this method, we observed that, in CMT2B RAB7 mutants, autophagosomes had a reduced fusion rate to lysosomes as compared to $RAB7^{WT}$, while constitutive active $RAB7^{Q67L}$ increased this rate and dominant negative $RAB7^{T22N}$ strongly impaired it (**Fig. 3**).

In order to validate data obtained on transfected HeLa cells, we next isolated and cultured skin fibroblasts from a CMT2B patient carrying the $RAB7^{V162M}$ mutation and from a healthy donor.[9] Again, we evaluated the colocalization rate between RAB7 and LC3B in control and

CMT2B skin fibroblasts and observed a reduction of colocalization in CMT2B cells compared to control cells (~57%, ~68% and ~50% in full medium, starvation and upon bafilomycin A_1 treatment, respectively; **Fig. 4A and 4B**), consistent with data obtained in HeLa cells (**Fig. 1A**).

Immunofluorescence analysis also revealed that the number of LC3B-positive vesicles was significantly reduced in CMT2B fibroblasts in each of the conditions tested and, in particular, the autophagic flux was significantly decreased in CMT2B fibroblasts (**Fig. 4A, 4C and 4D**). As a further confirmation, we also analyzed LC3B and RAB7 in fibroblasts by immunoblotting. In CMT2B cells, the autophagic flux was clearly reduced (**Fig. 5A and 5B**). Comparison of immunofluorescence and immunoblotting data showed that, while fewer LC3 vesicles were detected by immunofluorescence in CMT2B fibroblasts grown in full medium (**Fig. 4A, C**), immunoblotting in the same conditions revealed an increase of LC3B-II (**Fig. 5A and 5B**). However, it is worth noting that quantification of the autophagic flux in both cases demonstrated a strong inhibition (**Fig. 4D, 5C**), and that differences detected in full medium could be due to the different antibodies employed and to the detection limits of fluorescence microscopy. The inhibition of the autophagic flux in CMT2B fibroblasts was also evident both by starving cells in the absence or presence of bafilomycin A_1 (**Fig. 5D-F**) and by monitoring SQSTM1 and GABARAP-II after a long treatment with bafilomycin A_1 (**Fig. 5G-K**). Overall, our data, therefore, indicate a negative role of CMT2B mutations on autophagy while, at variance, the parallel endocytic pathway seems to be positively affected by the presence of the $RAB7^{V162M}$ mutant as degradation of TFRC (transferrin receptor) is increased (**Fig. S4**), confirming previous studies in different animal models (*Drosophila*, zebrafish) showing that

CMT2B mutants could behave both as inhibitory and as active proteins, depending on the kinetic requirements of the processes controlled by RAB7 (see, also, the Introduction).[17-19]

The role of RAB7 in autophagy has been extensively investigated and its function has been clearly correlated to autophagosome maturation and late endosome fusion with autophagic vesicles and lysosomes.[12,41,42] However, to verify that indeed CMT2B mutations in this gene do not affect also early phases of autophagosomal biogenesis, we evaluated the expression of the ATG12–ATG5 complex upon prolonged serum starvation.[38,39,43] Interestingly, ATG12–ATG5 levels similarly increased in normal and CMT2B fibroblasts, indicating that autophagosomal biogenesis was not affected by the RAB7^{V162M} mutation (**Fig. 6A-C**). As an additional confirmation of this result, we also monitored the formation of ATG5 and ATG12 puncta in starved cells, which is another marker for autophagosomal biogenesis.[38,39,43-45] Indeed, normal and CMT2B fibroblasts showed a similar amount of ATG5 and ATG12 puncta per cell, both in full medium and in starved cells (**Fig. 6D-G**), further supporting the idea that RAB7^{V162M} mutation does not affect autophagosomal biogenesis but acts in later steps of autophagosome maturation.

Discussion

Altogether, our results clearly indicate a reduction of CMT2B-causing RAB7 mutant localization on autophagic vesicles compared to the wild-type protein, suggesting functional consequences on autophagy, based on the important role of RAB7 in this process.[35,42,46-48] Indeed, by first using a

HeLa model cell system, we demonstrate that, different from the wild-type protein, these mutants fail to increase the number of autophagosomes both in basal conditions and after stimulation, behaving similarly to the dominant negative and functionally impaired RAB7^{T22N} mutant. Still, while model cell lines are widely used as easily manageable tools to understand molecular mechanisms involved in a wide variety of cellular phenomena, they do not necessarily fully recapitulate the biological conditions of affected cells *in vivo*. Indeed, while cells of CMT2B-affected individuals have one wild-type and one mutated allele, HeLa cells encode 3 functional copies of RAB7,[49] thus probably reducing the overall effect of mutated RAB7 exogenous expression. Hence, the possibility to analyze CMT2B patient's skin fibroblasts, carrying the RAB7^{V162M} mutation together with only 1 wild-type allele, allowed us to obtain more convincing results, in the precise cellular conditions in which the disease develops. Importantly, as demonstrated in HeLa cells, also in CMT2B fibroblasts colocalization of the mutated RAB7 protein with LC3B was very limited (~20%) and the number of LC3B-positive organelles was strongly reduced compared to control fibroblasts, in all conditions, clearly demonstrating that, in affected cells, the autophagic flux is inhibited. Immunofluorescence data obtained in patients' cells were also confirmed by western blot analysis of LC3B, SQSTM1 and GABARAP demonstrating an inhibition of the autophagic flux. Overall, experiments with patients' fibroblasts confirmed and reinforced our HeLa cell data and supported a model in which specific mutations in the RAB7 proteins represent a strong limiting factor for basal and induced autophagy in affected individuals, suggesting a reduced ability of mutated cells to respond to intra- and extracellular stimuli through activation of autophagy. In this context, it is important to note that in CMT2B cells degradation of TFRC was increased compared to control cells (**Fig.**

S4), similar to what we previously observed for EGFR (epidermal growth factor receptor) by transiently overexpressing the mutant in HeLa cells, although data were not statistically significant probably because of transient transfection efficiency variations between experiments.[14] Therefore, the RAB7^{V162M} mutant seems to have a different impact on endocytosis and autophagy and these results confirm that, although endosomal and autophagosomal maturation processes share many machinery components, they also display important differences and thus can be differentially regulated.[50,51] Clearly, further work is necessary to clarify the impact of CMT2B-causing mutant proteins on the endocytic pathway.

Autophagy is an essential process to eliminate cellular waste and, in post-mitotic cells such as neurons, failure of this process may cause accumulation of protein aggregates and, ultimately, lead to cell damage.[52] Indeed, neurons have very high and efficient basal autophagic activity and altered autophagy is now recognized as an important cause of neuronal degeneration both in the central and peripheral nervous system.[52-56] Axons and dendrites are particularly sensitive to accumulation of protein aggregates or damaged organelles and a growing body of evidence indicates that altered (both increased or inhibited) autophagy can lead to axonal and/or dendrite degeneration.[57-60] In addition, autophagy is induced after axonal damage in order to halt axonal degeneration.[61,62] Therefore, the impaired ability of CMT2B-causing RAB7 mutant proteins to induce autophagy could limit this important neuroprotective mechanism and, in the long term, support the establishment of CMT2B disease.

In conclusion, our data indicate that CMT2B mutations strongly affect cellular autophagic flux and suggest that inhibition of autophagy caused by expression of altered RAB7 proteins could be the cause of increased axonal degeneration leading to the neuropathy. This

information, therefore, suggests that the possibility of targeting autophagy may represent a potential approach to improve conditions of affected individuals, while taking advantage of assays for scoring autophagy (such as the described ratiometric flow cytometry flux assay) to rapidly evaluate, in vitro, the extent of the damage imposed by CMT2B-causing mutations and possibly select and guide forthcoming therapeutic options.

Materials and Methods

Isolation of human fibroblasts

After informed consent for pathological diagnosis, residual tissue specimens were collected following a biobanking standard operating procedure.[63] The samples were anonymously encoded to protect patient confidentiality and used under protocols approved by the Azienda Ospedaliera Universitaria "Federico II" Ethics Committee (Ethical Committee Approval Protocol #107/05). Aliquots of fresh tissue specimens were minced in small fragments (less than 1 mm^3), in a sterile environment and processed to obtain primary cultures of mesenchymal cells, as previously reported.[64] Tissue digestion was carried out at 37°C, for 2-4 h in a solution of type IV collagenase, 1 mg/mL (Sigma-Aldrich, 10103586001), containing 40 mg/mL bovine serum albumin (Sigma-Aldrich, A7979), 2 mg/mL glucose (Sigma-Aldrich, G7021), 100 U/ml penicillin and 100 mg/ml streptomycin (Sigma-Aldrich, P0781), 50 mg/l gentamicin (Sigma-Aldrich, G1397), 1.25 mg/l of Fungizone (Gibco, 15240-062). The samples were then extensively rinsed with phosphate-buffered saline (PBS; Oxoid, BR0014G) and suspended in standard culture media supplemented with 10% fetal bovine serum (FBS; Gibco, 12763-025). After 3 cycles of centrifugation, cells were allowed to attach overnight in Dulbecco minimal

essential medium (DMEM; Sigma-Aldrich, D6429), supplemented with 2 mM glutamine (Sigma-Aldrich, G7513), 100 U/ml penicillin and 100 mg/ml streptomycin, 15 mM HEPES (Sigma-Aldrich, H0887), 20% fetal bovine serum. Cells were cultured in 6-well plates at 37°C in a humidified atmosphere of 5% CO_2. The medium was renewed twice weekly.

Patient and control individual

Skin fibroblasts were obtained from the patient III.7 of the first identified Italian family affected by CMT2B, a 46-year old man, whose clinical history and symptoms have been already described.[9] Cells were also obtained from a healthy control individual age and sex matched.

Cells and culture conditions

Normal dermal human fibroblasts and dermal fibroblasts derived from a CMT2B patient were maintained in DMEM (Euroclone, ECB7501L) supplemented with 20% FBS (Euroclone, EUS0180L), 2 mM L-glutamine (Euroclone, ECB3000D), 100 units/ml penicillin-streptomycin (Euroclone, ECB3001D) at 37°C in an atmosphere of 5% CO_2:air. HeLa cells were maintained as previously described.[65] Briefly, they were cultured in DMEM as just described, except that 10% FBS was used. For immunofluorescence experiments cells were seeded on coverslips placed in 12-well plates; $5x10^4$ HeLa cells and $5x10^3$ fibroblasts were seeded in each well. For western blot and cytofluorometric analysis, $2x10^5$ HeLa cells were seeded in 6-well plates and $3x10^5$ fibroblast cells were seeded in 10-cm dishes. HeLa cells were transfected using Lipofectamine LTX (Life Technologies, 15338500) with the indicated plasmids (500 ng for 12-

well and 1000 ng for 6-well) 24 h before harvesting for western blot analysis and 48 h before fixing for immunofluorescence.[66]

Plasmids

Plasmids encoding HA-tagged RAB7^{WT} and the dominant negative RAB7^{T22N}, the constitutively active RAB7^{Q67L} and the CMT2B-causing RAB7^{L129F}, RAB7^{K157N}, RAB7^{N161T}, and RAB7^{V162M} mutant proteins, have been previously described.[14,15] The pcDNA3-HA plasmid was constructed by inserting a DNA sequence coding for a 2xHA-tag into the KpnI restriction site of the pCDNA3.1 (Invitrogen, V79020) and it was used as empty vector in control transfections. pBABE-puro mCherry-EGFP-LC3B was a gift from Jayanta Debnath (Addgene, 22418).[67]

Reagents and antibodies

Bafilomycin A_1 (Santa Cruz Biotechnology, sc-201550) was dissolved in DMSO. Hanks medium (ECB4006L), used as starvation medium, was obtained from Euroclone. For western blot analysis the following primary antibodies were used: anti-RAB7 (Santa Cruz Biotechnology, sc-376362), anti-HA (Covance, MMS-101R), anti-LC3B (Nanotools, 0231-1000), anti-GABARAP (MBL, M135-3), anti-SQSTM1/p62 (BD Biosciences, 610833), anti-tubulin/TUBA1A (Sigma-Aldrich, T5168) and anti-MAPK1/ERK2 (Santa Cruz Biotechnology, sc-154). For confocal immunofluorescence microscopy experiments, the following primary antibodies were used: anti-HA (Roche, 11867423001), anti-LC3B (MBL, M152-3), anti-RAB7 (Cell Signaling Technology, 9367), anti-ATG12 (Cell Signaling Technology, 2010) and anti-ATG5 (Sigma-Aldrich, A0731). The following secondary antibodies were used for western blot

experiments: anti-mouse (Santa Cruz Biotechnology, sc-2004) and anti-rabbit (Santa Cruz Biotechnology, sc-2005) HRP-conjugated IgGs. The following secondary antibodies were used for confocal microscopy experiments: anti-mouse Alexa Fluor 488-conjugated (Life Technologies, A21202), anti-rabbit Alexa Fluor 488-conjugated (Life Technologies, A21206), anti-mouse Alexa Fluor 555-conjugated (Life Technologies, A31570), anti-rabbit Alexa Fluor 555-conjugated (Life Technologies, A31572), and anti-rat Alexa Fluor 594-conjugated (Life Technologies, A21209).

Western blot analysis

Total lysates were obtained and treated as previously described.[68] Briefly, washed cellular pellet fractions were resuspended in MAPK lysis buffer made of 20 mM HEPES (PAA, S11001), pH 7.5, 10 mM EGTA (Sigma-Aldrich, E4378), 40 mM beta-glycerophosphate (Sigma-Aldrich, G6501), 1% NP-40 (Sigma-Aldrich, I3021), 2.5 mM $MgCl_2$ (Sigma-Aldrich, M2670), 2 mM orthovanadate (Sigma-Aldrich, S6508), 2 mM NaF (Carlo Erba, 7681494), 1 mM DTT (IBI, IB21040), Roche protease inhibitors cocktail (Roche Diagnostics, 05056489001). Proteins were quantified by the Bradford assay and, before loading, 5X Laemmli sample buffer was added to the lysates, which were next incubated for 5 min at 95°C. Alternatively cells were directly lysed in 1X Laemmli. Lysates were loaded on SDS-PAGE polyacrylamide gels, transferred to Immobilon-P PVDF membrane (Millipore, IPVH00010), probed with the appropriate antibodies, and detected using enhanced chemoluminescence (ECL Prime; GE Healthcare, RPN2232). Images were then acquired with a LAS 4000 imager (GE Healthcare, Italy, Milan).

Densitometric analysis of western blots was performed with NIH ImageJ 1.43u (National Institutes of Health).

Immunofluorescence

Cells were cultured and treated as previously described.[65] Briefly, they were washed with PBS, then fixed with 4% paraformaldehyde (Sigma-Aldrich, 47608) in 1X PBS for 20 min and permeabilized with 0.2% Triton X-100 (Sigma-Aldrich, T8787) for 10 min or 100 μg/ml digitonin solution (Life Technologies, BN2006) for 20 min. Permeabilized cells were incubated with the appropriate primary antibodies for 1 h, washed 3 times with 1X PBS, incubated for 30 min with appropriate secondary antibodies and then washed again 3 times in 1X PBS. Nuclei were stained with a solution of 1.5 μM of 4',6-diamidino-2-phenylindole (DAPI; Sigma-Aldrich, D9542) in PBS for 5 min. Coverslips were mounted in Fluorescence Mounting Medium (Dako, S3023). Samples were visualized on a TSC SP5 confocal microscope (Leica Microsystems, Germany, Mannheim) installed on an inverted LEICA DMI 6000CS microscope (Leica Microsystems, Germany, Mannheim) and equipped with an oil immersion PlanApo 63X 1.4 NA objective. Images were acquired using the LAS AF acquisition software (Leica Microsystems).

Flow cytometry

Cells treated with full medium or starvation medium were harvested and resuspended in the same medium of the treatment for FACS analysis to avoid autophagic flux changes. EGFP and mCherry fluorescence signal were evaluated by flow cytometry in LSR-II FACS (BD Biosciences, Italy, Milan), equipped with 488-nm and 561-nm laser according to Gump and

Thorburn.[40] A derived parameter with the ratio between mCherry and EGFP signal was generated to measure the autophagic flux. For each sample at least $5x10^5$ cells were acquired for each experiment.

Dot count and colocalization rate

For the LC3B-positive dot count, we performed intensitometric analysis of fluorescence using the Quantitation Module of Volocity software (PerkinElmer Life Science).[69] LC3B dots area, Pearson correlation and colocalization rate were also measured by the Quantitation Module of Volocity software. Dot count and colocalization rate were subjected to statistical analysis. Measures were obtained by analyzing at least 400 cells/sample for at least 3 different experiments. Significance (*P* value) was assessed by one-way ANOVA test.

TFRC degradation

Cells were incubated with 50 μg/ml cycloheximide (Sigma-Aldrich, C7698) up to 8 h and then lysed. Lysates were subjected to western blot analysis with anti-TFRC/transferrin receptor antibody (mouse monoclonal G1/221/12 developed by H.P. Hauri and obtained from the Developmental Studies Hybridoma Bank, created by the NICHD of the NIH and maintained at The University of Iowa, Department of Biology, Iowa City, IA, USA) to follow TFRC degradation.

Acknowledgements

The financial support of Telethon-Italy (Grant GGP16037 to C.B.) and AIRC (Associazione Italiana per la Ricerca sul Cancro, Investigator Grant 2016 N. 19068 to C.B.), is gratefully acknowledged. We thank TLS Foundation in Siena for providing infrastructure and instrumentation for performing several experiments.

Disclosure of Potential Conflicts of Interest

The authors declare that they have no conflicting financial interest.

References

1. Bucci C, Bakke O, Progida C. Charcot-Marie-Tooth disease and intracellular traffic. Prog Neurobiol 2012; 99:191-225.
2. Timmerman V, Strickland AV, Züchner S. Genetics of Charcot-Marie-Tooth (CMT) Disease within the Frame of the Human Genome Project Success. Genes (Basel) 2014; 5:13-32.
3. Meggouh F, Bienfait HM, Weterman MA, de Visser M, Baas F. Charcot-Marie-Tooth disease due to a de novo mutation of the RAB7 gene. Neurology 2006; 67:1476-8.
4. Houlden H, King RH, Muddle JR, Warner TT, Reilly MM, Orrell RW, Ginsberg L. A novel RAB7 mutation associated with ulcero-mutilating neuropathy. Ann Neurol 2004; 56:586-90.
5. Verhoeven K, De Jonghe P, Coen K, Verpoorten N, Auer-Grumbach M, Kwon JM, FitzPatrick D, Schmedding E, De Vriendt E, Jacobs A, et al. Mutations in the small GTP-ase late endosomal protein RAB7 cause Charcot-Marie-Tooth type 2B neuropathy. Am J Hum Genet 2003; 72:722-7.
6. Wang X, Han C, Liu W, Wang P, Zhang X. A novel RAB7 mutation in a Chinese family with Charcot-Marie-Tooth type 2B disease. Gene 2014; 534:431-4.
7. Bucci C, De Luca M. Molecular basis of Charcot-Marie-Tooth type 2B disease. Biochem Soc Trans 2012; 40:1368-72.
8. Cogli L, Piro F, Bucci C. Rab7 and the CMT2B disease. Biochem Soc Trans 2009; 37:1027-31.

9. Manganelli F, Pisciotta C, Provitera V, Taioli F, Iodice R, Topa A, Fabrizi GM, Nolano M, Santoro L. Autonomic nervous system involvement in a new CMT2B family. J Peripher Nerv Syst 2012; 17:361-4.
10. Bucci C, Thomsen P, Nicoziani P, McCarthy J, van Deurs B. Rab7: a key to lysosome biogenesis. Mol Biol Cell 2000; 11:467-80.
11. Wang T, Ming Z, Xiaochun W, Hong W. Rab7: role of its protein interaction cascades in endo-lysosomal traffic. Cell Signal 2011; 23:516-21.
12. Hyttinen JM, Niittykoski M, Salminen A, Kaarniranta K. Maturation of autophagosomes and endosomes: a key role for Rab7. Biochim Biophys Acta 2013; 1833:503-10.
13. Vitelli R, Santillo M, Lattero D, Chiariello M, Bifulco M, Bruni C, Bucci C. Role of the small GTPase Rab7 in the late endocytic pathway. J Biol Chem 1997; 272:4391-7.
14. Spinosa MR, Progida C, De Luca A, Colucci AMR, Alifano P, Bucci C. Functional characterization of Rab7 mutant proteins associated with Charcot-Marie-Tooth type 2B disease. J Neurosci 2008; 28:1640-8.
15. De Luca A, Progida C, Spinosa MR, Alifano P, Bucci C. Characterization of the Rab7K157N mutant protein associated with Charcot-Marie-Tooth type 2B. Biochem Biophys Res Commun 2008; 372:283-7.
16. McCray BA, Skordalakes E, Taylor JP. Disease mutations in Rab7 result in unregulated nucleotide exchange and inappropriate activation. Hum Mol Genet 2010; 19:1033-47.
17. Cherry S, Jin EJ, Ozel MN, Lu Z, Agi E, Wang D, Jung WH, Epstein D, Meinertzhagen IA, Chan CC, et al. Charcot-Marie-Tooth 2B mutations in rab7 cause dosage-dependent neurodegeneration due to partial loss of function. Elife 2013; 2:e01064.

18. Janssens K, Goethals S, Atkinson D, Ermanoska B, Fransen E, Jordanova A, Auer-Grumbach M, Asselbergh B, Timmerman V. Human Rab7 mutation mimics features of Charcot-Marie-Tooth neuropathy type 2B in Drosophila. Neurobiol Dis 2014; 65:211-9.
19. Ponomareva OY, Eliceiri KW, Halloran MC. Charcot-Marie-Tooth 2b associated Rab7 mutations cause axon growth and guidance defects during vertebrate sensory neuron development. Neural Dev 2016; 11:2.
20. Saxena S, Bucci C, Weis J, Kruttgen A. The small GTPase Rab7 controls the endosomal trafficking and neuritogenic signaling of the nerve growth factor receptor TrkA. J Neurosci 2005; 25:10930-40.
21. Kawauchi T, Sekine K, Shikanai M, Chihama K, Tomita K, Kubo K, Nakajima K, Nabeshima Y, Hoshino M. Rab GTPases-dependent endocytic pathways regulate neuronal migration and maturation through N-cadherin trafficking. Neuron 2010; 67:588-602.
22. Cogli L, Progida C, Lecci R, Bramato R, Krüttgen A, Bucci C. CMT2B-associated Rab7 mutants inhibit neurite outgrowth. Acta Neuropathol 2010; 120:491-501.
23. Deinhardt K, Salinas S, Verastegui C, Watson R, Worth D, Hanrahan S, Bucci C, Schiavo G. Rab5 and Rab7 control endocytic sorting along the axonal retrograde transport pathway. Neuron 2006; 52:293-305.
24. Yamauchi J, Torii T, Kusakawa S, Sanbe A, Nakamura K, Takashima S, Hamasaki H, Kawaguchi S, Miyamoto Y, Tanoue A. The mood stabilizer valproic acid improves defective neurite formation caused by Charcot-Marie-Tooth disease-associated mutant Rab7 through the JNK signaling pathway. J Neurosci Res 2010; 88:3189-97.

25. Shea TB, Beermann ML, Fischer I. Transient requirement for vimentin in neuritogenesis: intracellular delivery of anti-vimentin antibodies and antisense oligonucleotides inhibit neurite initiation but not elongation of existing neurites in neuroblastoma. J Neurosci Res 1993; 36:66-76.

26. Dubey M, Hoda S, Chan WK, Pimenta A, Ortiz DD, Shea TB. Reexpression of vimentin in differentiated neuroblastoma cells enhances elongation of axonal neurites. J Neurosci Res 2004; 78:245-9.

27. Cogli L, Progida C, Bramato R, Bucci C. Vimentin phosphorylation and assembly are regulated by the small GTPase Rab7a. Biochim Biophys Acta 2013; 1833:1283-93.

28. Cogli L, Progida C, Thomas CL, Spencer-Dene B, Donno C, Schiavo G, Bucci C. Charcot-Marie-Tooth type 2B disease-causing RAB7A mutant proteins show altered interaction with the neuronal intermediate filament peripherin. Acta Neuropathol 2013; 25:257-72.

29. Toth C, Shim SY, Wang J, Jiang Y, Neumayer G, Belzil C, Liu WQ, Martinez J, Zochodne D, Nguyen MD. Ndel1 promotes axon regeneration via intermediate filaments. PLoS One 2008; 3:e2014.

30. Margiotta A, Progida C, Bakke O, Bucci C. Rab7a regulates cell migration through Rac1 and vimentin. Biochim Biophys Acta 2017; 1864:367-81.

31. Margiotta A, Bucci C. Role of Intermediate Filaments in Vesicular Traffic. Cells 2016; 5:E20.

32. Jiang P, Mizushima N. Autophagy and human diseases. Cell Res 2014; 24:69-79.

33. Damme M, Suntio T, Saftig P, Eskelinen E-L. Autophagy in neuronal cells: general principles and physiological and pathological functions. Acta Neuropathologica 2014; 129:337-62.

34. Nikoletopoulou V, Papandreou M, Tavernarakis N. Autophagy in the physiology and pathology of the central nervous system. Cell Death Differ 2014; 22:398-407.

35. Jager S, Bucci C, Tanida I, Ueno T, Kominami E, Saftig P, Eskelinen EL. Role for Rab7 in maturation of late autophagic vacuoles. J Cell Sci 2004; 117:4837-48.

36. Eskelinen EL. Maturation of autophagic vacuoles in Mammalian cells. Autophagy 2005; 1:1-10.

37. Carroll B, Mohd-Naim N, Maximiano F, Frasa MA, McCormack J, Finelli M, Thoresen SB, Perdios L, Daigaku R, Francis RE, et al. The TBC/RabGAP Armus coordinates Rac1 and Rab7 functions during autophagy. Dev Cell 2013; 25:15-28.

38. Jin M, Klionsky DJ. Regulation of autophagy: modulation of the size and number of autophagosomes. FEBS Lett 2014; 588:2457-63.

39. Klionsky DJ, Abdelmohsen K, Abe A, Abedin MJ, Abeliovich H, Acevedo Arozena A, Adachi H, Adams CM, Adams PD, Adeli K, et al. Guidelines for the use and interpretation of assays for monitoring autophagy (3rd edition). Autophagy 2016; 12:1-222.

40. Gump JM, Thorburn A. Sorting cells for basal and induced autophagic flux by quantitative ratiometric flow cytometry. Autophagy 2014; 10:1327-34.

41. Wen H, Zhan L, Chen S, Long L, Xu E. Rab7 may be a novel therapeutic target for neurologic diseases as a key regulator in autophagy. J Neurosci Res 2017; doi: 10.1002/jnr.24034.

42. Guerra F, Bucci C. Multiple Roles of the Small GTPase Rab7. Cells 2016; 5:E34.

43. Koyama-Honda I, Itakura E, Fujiwara TK, Mizushima N. Temporal analysis of recruitment of mammalian ATG proteins to the autophagosome formation site. Autophagy 2013; 9:1491-9.

44. Sakoh-Nakatogawa M, Matoba K, Asai E, Kirisako H, Ishii J, Noda NN, Inagaki F, Nakatogawa H, Ohsumi Y. Atg12-Atg5 conjugate enhances E2 activity of Atg3 by rearranging its catalytic site. Nat Struct Mol Biol 2013; 20:433-9.

45. Carlsson SR, Simonsen A. Membrane dynamics in autophagosome biogenesis. J Cell Sci 2015; 128:193-205.

46. Hegedűs K, Takáts S, Boda A, Jipa A, Nagy P, Varga K, Kovács AL, Juhász G. The Ccz1-Mon1-Rab7 module and Rab5 control distinct steps of autophagy. Mol Biol Cell 2016; 27:3132-42.

47. Roy SG, Stevens MW, So L, Edinger AL. Reciprocal effects of rab7 deletion in activated and neglected T cells. Autophagy 2013; 9:1009-23.

48. Lizaso A, Tan KT, Lee YH. β-adrenergic receptor-stimulated lipolysis requires the RAB7-mediated autolysosomal lipid degradation. Autophagy 2013; 9:1228-43.

49. Landry JJ, Pyl PT, Rausch T, Zichner T, Tekkedil MM, Stütz AM, Jauch A, Aiyar RS, Pau G, Delhomme N, et al. The genomic and transcriptomic landscape of a HeLa cell line. G3 (Bethesda) 2013; 3:1213-24.

50. Ganley IG, Wong PM, Jiang X. Thapsigargin distinguishes membrane fusion in the late stages of endocytosis and autophagy. Autophagy 2011; 7:1397-9.

51. Ganley IG, Wong PM, Gammoh N, Jiang X. Distinct autophagosomal-lysosomal fusion mechanism revealed by thapsigargin-induced autophagy arrest. Mol Cell 2011; 42:731-43.

52. Maday S. Mechanisms of neuronal homeostasis: Autophagy in the axon. Brain Research 2016; 1649:143-50.

53. Boland B, Nixon RA. Neuronal macroautophagy: from development to degeneration. Mol Aspects Med 2006; 27:503-19.

54. Nixon RA. The role of autophagy in neurodegenerative disease. Nat Med 2013; 19:983-97.

55. Menzies FM, Fleming A, Rubinsztein DC. Compromised autophagy and neurodegenerative diseases. Nat Rev Neurosci 2015; 16:345-57.

56. Wang D, Chan CC, Cherry S, Hiesinger PR. Membrane trafficking in neuronal maintenance and degeneration. Cell Mol Life Sci 2013; 70:2919-34.

57. Yang Y, Coleman M, Zhang L, Zheng X, Yue Z. Autophagy in axonal and dendritic degeneration. Trends Neurosci 2013; 36:418-28.

58. Kosacka J, Nowicki M, Blüher M, Baum P, Stockinger M, Toyka KV, Klöting I, Stumvoll M, Serke H, Bechmann I, et al. Increased autophagy in peripheral nerves may protect Wistar Ottawa Karlsburg W rats against neuropathy. Exp Neurol 2013; 250:125-35.

59. Ribas VT, Schnepf B, Challagundla M, Koch JC, Bähr M, Lingor P. Early and sustained activation of autophagy in degenerating axons after spinal cord injury. Brain Pathol 2015; 25:157-70.

60. Launay N, Aguado C, Fourcade S, Ruiz M, Grau L, Riera J, Guilera C, Giròs M, Ferrer I, Knecht E, et al. Autophagy induction halts axonal degeneration in a mouse model of X-adrenoleukodystrophy. Acta Neuropathol 2015; 129:399-415.

61. Casas C, Isus L, Herrando-Grabulosa M, Mancuso FM, Borrás E, Sabidó E, Forés J, Aloy P. Network-based proteomic approaches reveal the neurodegenerative, neuroprotective and pain-related mechanisms involved after retrograde axonal damage. Sci Rep 2015; 5:9185.
62. Hou H, Zhang L, Zhang L, Liu D, Xiong Q, Du H, Tang P. Acute spinal cord injury could cause activation of autophagy in dorsal root ganglia. Spinal Cord 2013; 51:679-82.
63. Nardone A, Cavaliere C, Corvigno S, Limite G, De Placido S, Veneziani BM. A banking strategy toward customized therapy in breast cancer. Cell Tissue Bank 2009; 10:301-8.
64. Leccia F, Nardone A, Corvigno S, Vecchio LD, De Placido S, Salvatore F, Veneziani BM. Cytometric and biochemical characterization of human breast cancer cells reveals heterogeneous myoepithelial phenotypes. Cytometry 2012; 81:960-72.
65. Colecchia D, Strambi A, Sanzone S, Iavarone C, Rossi M, Dall'Armi C, Piccioni F, Verrotti di Pianella A, Chiariello M. MAPK15/ERK8 stimulates autophagy by interacting with LC3 and GABARAP proteins. Autophagy 2012; 8:1724-40.
66. Rossi M, Colecchia D, Iavarone C, Strambi A, Piccioni F, Verrotti di Pianella A, Chiariello M. Extracellular signal-regulated kinase 8 (ERK8) controls estrogen-related receptor α (ERRα) cellular localization and inhibits its transcriptional activity. J Biol Chem 2011; 286:8507-22.
67. N'Diaye EN, Kajihara KK, Hsieh I, Morisaki H, Debnath J, Brown EJ. PLIC proteins or ubiquilins regulate autophagy-dependent cell survival during nutrient starvation. EMBO Rep 2009; 10:173-9.

68. Strambi A, Mori M, Rossi M, Colecchia D, Manetti F, Carlomagno F, Botta M, Chiariello M. Structure prediction and validation of the ERK8 kinase domain. PLoS One 2013; 8:e52011.

69. Rossi M, Colecchia D, Ilardi G, Acunzo M, Nigita G, Sasdelli F, Celetti A, Strambi A, Staibano S, Croce CM, et al. MAPK15 upregulation promotes cell proliferation and prevents DNA damage in male germ cell tumors. Oncotarget 2016; 7:20981-98.

Figure legends

Figure 1. Analysis of autophagy in HeLa cells expressing CMT2B-causing RAB7 mutant proteins. HeLa cells transfected for 48 h with empty vector or plasmids encoding HA-tagged $RAB7^{WT}$, $RAB7^{Q67L}$, $RAB7^{T22N}$ and CMT2B-causing RAB7 mutants ($RAB7^{L129F}$, $RAB7^{K157N}$, $RAB7^{N161T}$, $RAB7^{V162M}$), were incubated in full medium (FM) or starvation medium (ST) for 30 min, or in the presence of 100 nM bafilomycin A_1 (BAF) for 3 h. (**A**) The colocalization rate between RAB7 and LC3B was analyzed for the each different RAB7 isoform and for each condition (FM, ST, BAF). (**B**) The number of LC3B-positive dots per cell was evaluated for each sample. (**C**) The autophagic flux was calculated as the ratio of LC3B dots between BAF and FM of the same sample and normalized on empty vector. Quantification of results was performed by unbiased intensitometric analysis of fluorescence using the Quantitation Module of Volocity software.[69] Statistical analysis one-way ANOVA test was performed between the same conditions (FM, ST and BAF) selecting $RAB7^{WT}$ as the referring sample. All statistical comparisons are from the sample indicated with asterisks and $RAB7^{WT}$. Means ± SEM for each value are shown in the graphs (n=3). * = $p < 0.05$; ** = $p < 0.01$; *** = $p < 0.001$.

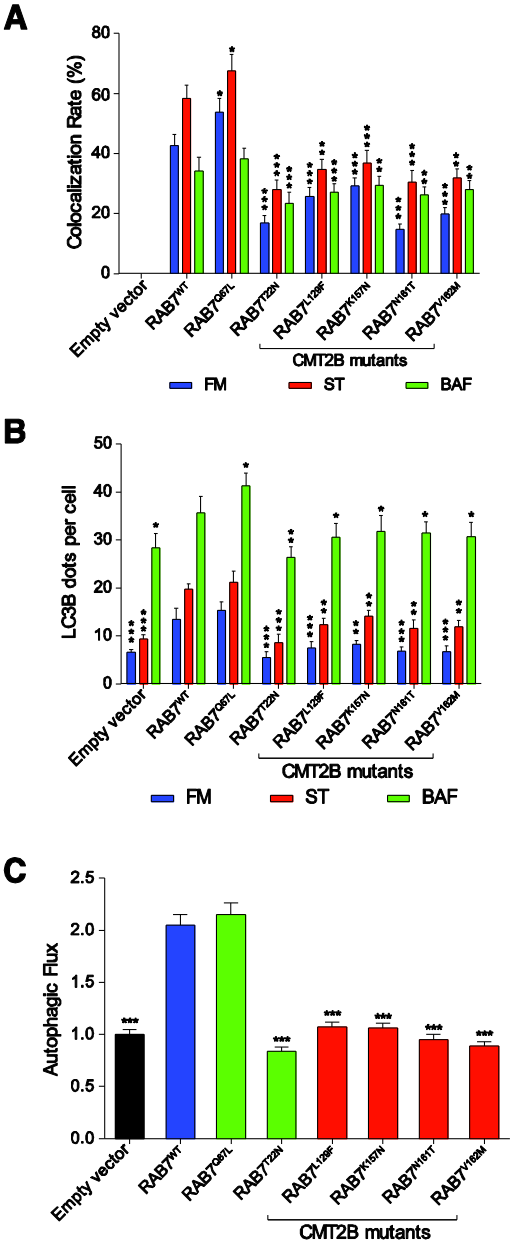

Fig. 1

ACCEPTED MANUSCRIPT

Figure 2. Analysis of autophagy in HeLa cells expressing CMT2B-causing RAB7 mutant proteins. HeLa cells transfected for 48 h with empty vector or plasmids encoding HA-tagged $RAB7^{WT}$, $RAB7^{Q67L}$, $RAB7^{T22N}$ and CMT2B-causing RAB7 mutants ($RAB7^{L129F}$, $RAB7^{K157N}$, $RAB7^{N161T}$, $RAB7^{V162M}$). Cells were incubated in full medium (FM) or starvation medium (ST) for 30 min, or in the presence of 100 nM bafilomycin A_1 (BAF) for 3 h. (**A**) Cells were incubated in full medium or starvation medium for 30 min, or in the presence of BAF for 3 h. Immunoblot of LC3B, HA-RAB7, endogenous RAB7 and MAPK1. Representative images from 3 independent experiments are shown (n=3). (**B**) Intensitometric analysis of LC3B and MAPK1 immunoblots shown in (**A**) were performed with NIH ImageJ. (**C**) The autophagic flux was calculated as the ratio of normalized LC3B-II between BAF and FM of the same sample. (**D**) Cells were incubated in full medium or in the presence of BAF for 24 h and next immunobloted for SQSTM1, GABARAP, HA-RAB7, endogenous RAB7 and MAPK1 proteins. Representative images from 3 independent experiments are shown (n=3). (**E**) Intensitometric analysis of SQSTM1, GABARAP and MAPK1 immunoblots was used to calculate the autophagic flux as the ratio of LC3B dots between BAF and FM of the same sample. Statistical analysis one-way ANOVA test was performed between the same conditions (FM, ST and BAF) selecting $RAB7^{WT}$ as the referring sample. All statistical comparisons are from the sample indicated with asterisks and $RAB7^{WT}$. Means ± SEM for each value are shown in the graphs. * = $p < 0.05$; ** = $p < 0.01$; *** = $p < 0.001$.

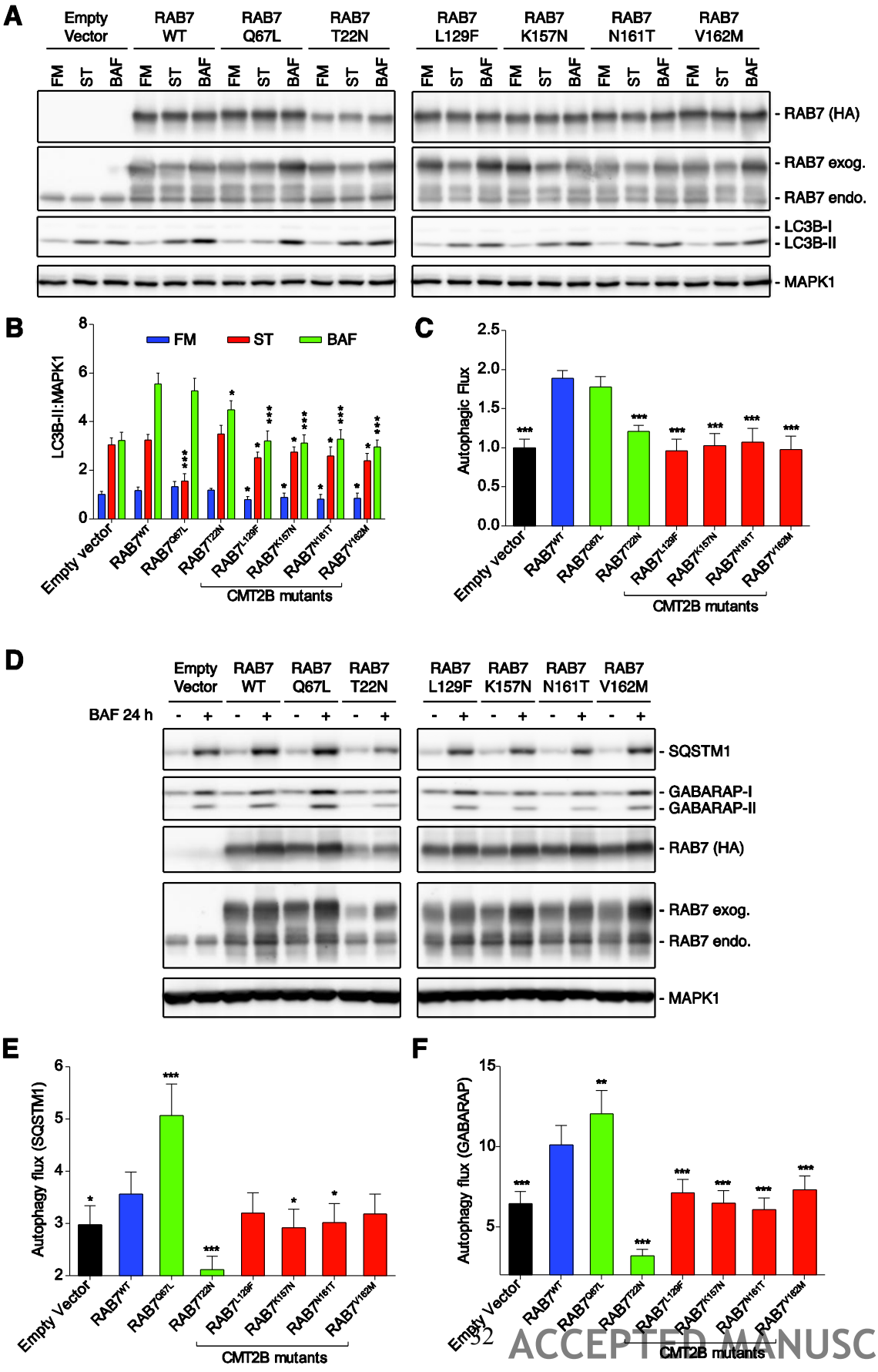

Fig. 2

Figure 3. Analysis of autophagic flux in EGFP-mCherry-LC3B HeLa cells expressing CMT2B-causing RAB7 mutant proteins. HeLa cells transfected for 48 h with empty vector or plasmids encoding HA-tagged $RAB7^{WT}$, $RAB7^{Q67L}$, $RAB7^{T22N}$ and CMT2B-causing RAB7 mutants ($RAB7^{L129F}$, $RAB7^{K157N}$, $RAB7^{N161T}$, $RAB7^{V162M}$), were incubated in full medium (FM) or starvation medium (ST) for 4 h. Scatter and singlet gates were used to eliminate debris, dead cells, and mitotic cells. For each experiment, voltages and gain on EGFP and mCherry detectors are set empirically on negative and positive controls to allow the best plot fit on the mCherry:EGFP ratio histogram. Statistical analysis one-way ANOVA test was performed between the same conditions (FM and ST) selecting $RAB7^{WT}$ as the referring sample. All statistical comparisons are from the sample indicated with asterisks and the corresponding $RAB7^{WT}$. Means ± SEM for each value are shown in the graphs. * = $p < 0.05$; ** = $p < 0.01$; *** = $p < 0.001$. (**A**) Graph shows the percentage of cells with high autophagic flux (measured as mCherry:EGFP ratio) in FM and ST for each sample. (**B**) Histograms plotting cell counts versus mCherry:EGFP ratio with a bar indicating the gate for high autophagic flux cell population. Representative images from 3 independent experiments are shown (n=3).

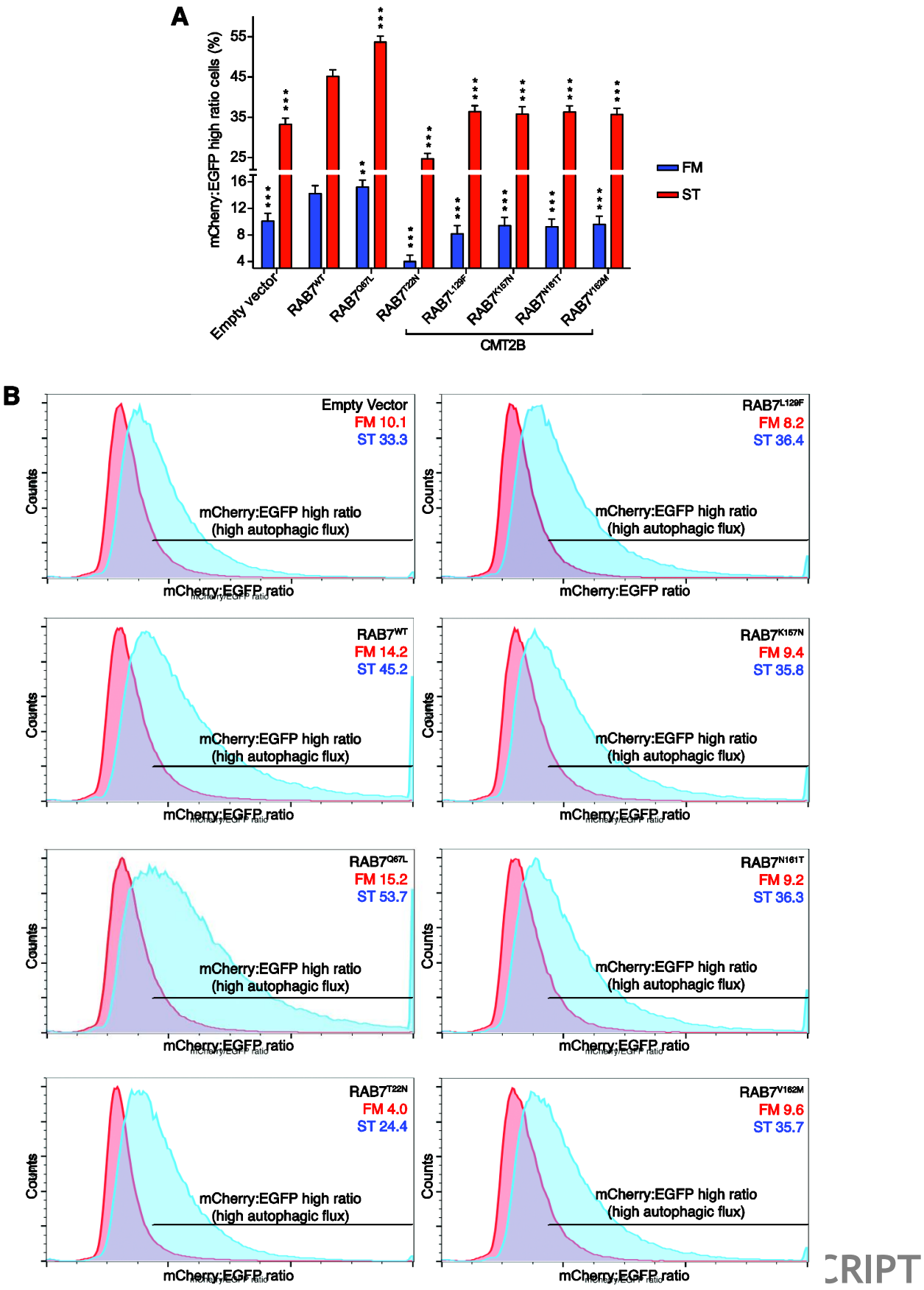

Fig.3

Figure 4. Analysis of autophagy in CMT2B fibroblasts. Normal dermal human fibroblasts (NDHF) and CMT2B patient-derived fibroblasts were incubated with full medium or starvation medium for 30 min, or incubated with 400 nM bafilomycin A_1 for 3 h. (**A**) Representative images (n=3) for NDHF and CMT2B fibroblasts labeled for LC3B (green), RAB7 (red) and nuclei (blue). White squares indicated the area enlarged in the zoom. (**B**) Colocalization rate between RAB7 and LC3B was analyzed for each condition (FM, ST, BAF). (**C**) The number of autophagosomes (scored as LC3B-positive dots) per cell was evaluated for each sample. (**D**) The autophagic flux was calculated as the ratio of LC3B dots between FM and BAF of the same sample. Statistical analysis was performed using one-way ANOVA test where normal fibroblasts were selected as referring sample for each condition (FM, ST and BAF). Means ± SEM for each value are shown in the graphs. * = $p < 0.05$; ** = $p < 0.01$; *** = $p < 0.001$. Scale bars are 10 μm for FM and BAF and 25 μm for ST.

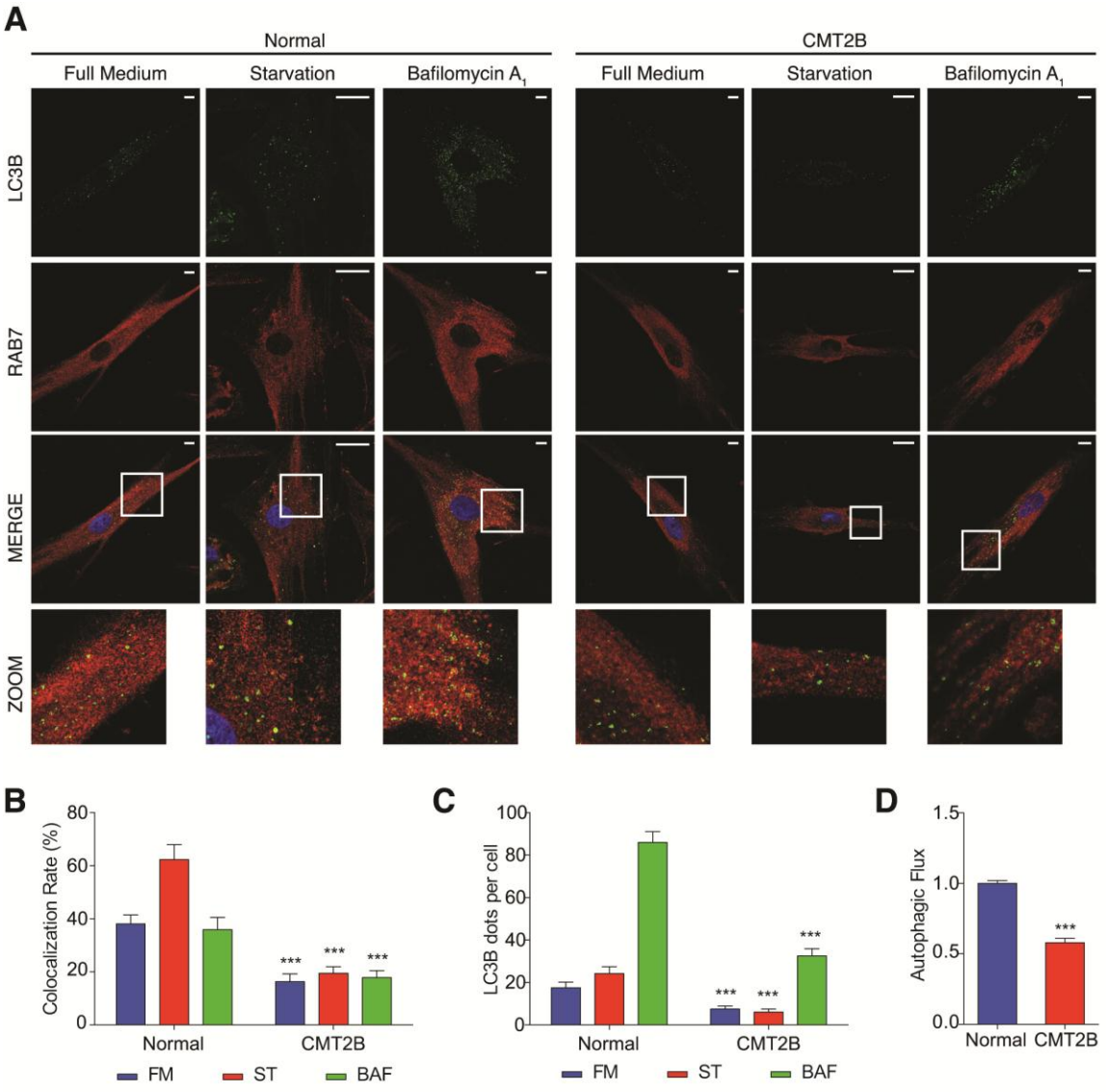

Fig. 4

Figure 5. Analysis of autophagy in CMT2B fibroblasts. (**A**) Normal dermal human fibroblasts and CMT2B patient derived fibroblasts were incubated with full medium (FM) or starvation medium (ST) for 30 min, or incubated with 400 nM bafilomycin A_1 (BAF) for 3 h. Immunoblot of LC3B, HA-RAB7 proteins and MAPK1. Representative images from 3 independent experiments are shown (n=3). (**B**) Intensitometric analysis of LC3B and MAPK1 immunoblots shown in (**A**) were performed with NIH ImageJ. (**C**) The autophagic flux was calculated as the ratio of normalized LC3B-II between BAF and FM of the same sample. (**D**) Normal dermal human fibroblasts and CMT2B patient-derived fibroblasts were incubated with starvation medium with or without 400 nM BAF for 3 h. Immunoblot of LC3B, RAB7 proteins and MAPK1. Representative images from 3 independent experiments are shown (n=3). (**E**) Intensitometric analysis of LC3B and MAPK1 immunoblots shown in (**D**) were performed with NIH ImageJ. The autophagic flux was calculated as the ratio of LC3B dots between BAF and FM of the same sample. (**F**) The autophagic flux was calculated as the ratio of normalized LC3B-II between BAF and FM of the same sample. (**G**) Normal dermal human fibroblasts and CMT2B patient derived fibroblasts were incubated with full medium or incubated with 400 nM BAF for 24 h. Immunoblot of SQSTM1, GABARAP, RAB7 and MAPK1 proteins. Representative images from 3 independent experiments are shown (n=3). (**H**) Intensitometric analysis of SQSTM1 and MAPK1 immunoblots shown in (**G**) were performed with NIH ImageJ. (**I**) The autophagic flux was calculated as the ratio of normalized SQSTM1 between BAF and FM of the same sample. (**J**) Intensitometric analysis of GABARAP-II and MAPK1 immunoblots shown in (**G**) were performed with NIH ImageJ. (**K**) The autophagic flux was calculated as the ratio of normalized GABARAP-II between BAF and FM of the same sample. Statistical analysis

was performed using one-way ANOVA test where normal fibroblasts were selected as referring sample for each condition (FM, ST and BAF). Means ± SEM for each value are shown in the graphs. * = $p < 0.05$; ** = $p < 0.01$; *** = $p < 0.001$.

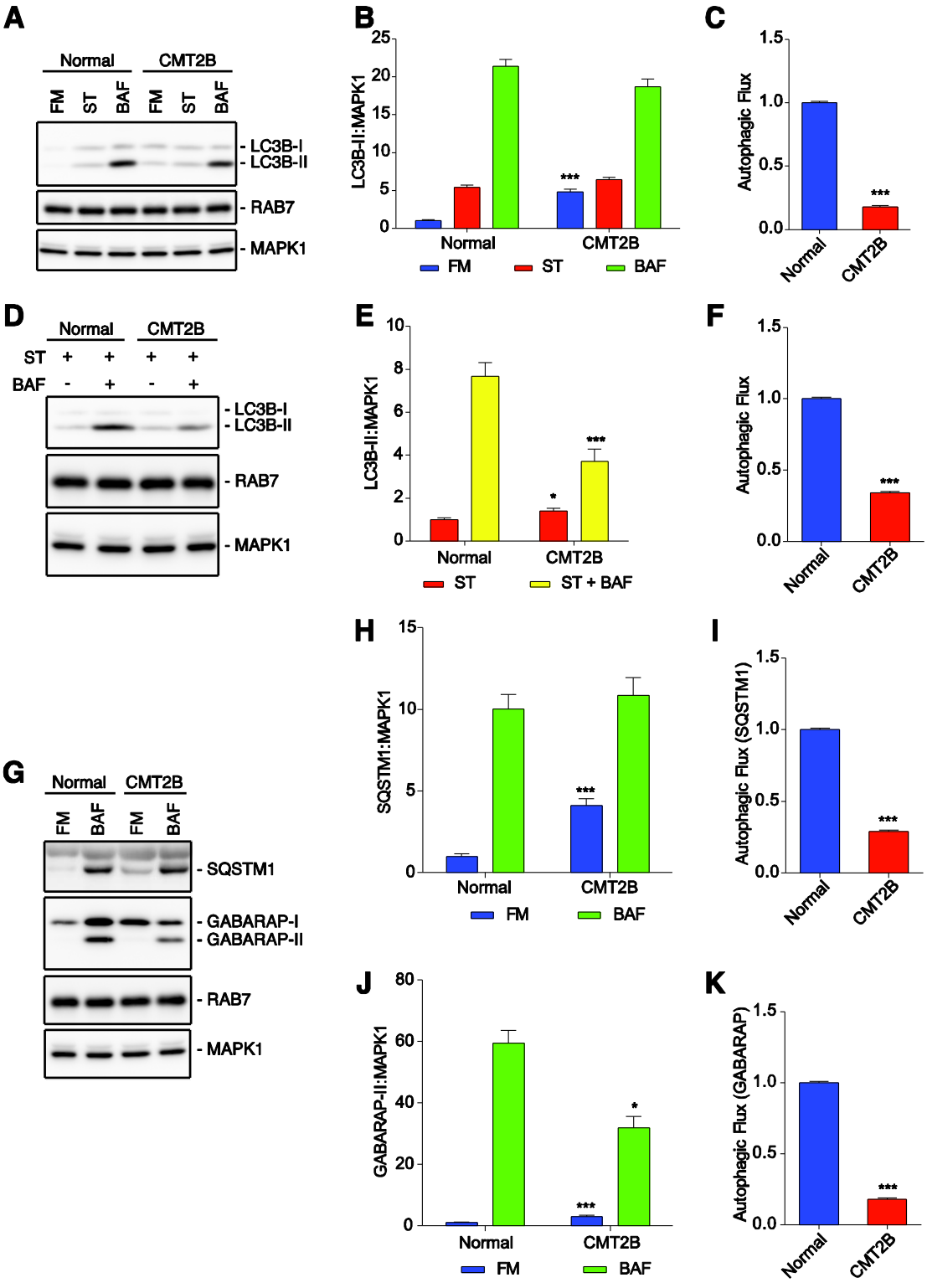

Fig.5

Figure 6. Analysis of autophagosome biogenesis in CMT2B fibroblasts. Statistical analysis was performed using one-way ANOVA test where normal fibroblasts were selected as referring sample for each condition (full medium [FM] and serum starved [ST]). Means ± SEM for each value are shown in the graphs. (**A**) Normal dermal human fibroblasts and CMT2B patient-derived fibroblasts were incubated with full medium or serum starved medium for 6 sec. Immunoblots of ATG5, ATG12 and MAPK1 proteins. Representative images from 3 independent experiments are shown (n=3). (**B**) Intensitometric analysis of ATG12–ATG5 complex (labeled with ATG5) and MAPK1 immunoblots shown in (**A**) were performed with NIH ImageJ. (**C**) Intensitometric analysis of ATG12–ATG5 complex (labeled with ATG12) and MAPK1 immunoblots shown in (**A**) were performed with NIH ImageJ. (**D**) Representative images (n=3) for NDHF and CMT2B fibroblasts labeled for ATG12 (green) and nuclei (blue). Scale bars are 25 μm. (**E**) The number of ATG12 puncta per cell was evaluated for each sample. (**F**) Representative images (n=3) for NDHF and CMT2B fibroblasts labeled for ATG5 (green) and nuclei (blue). (**G**) The number of ATG5 puncta per cell was evaluated for each sample. Scale bars are 25 μm except for starved CMT2B where they are 10 μm.

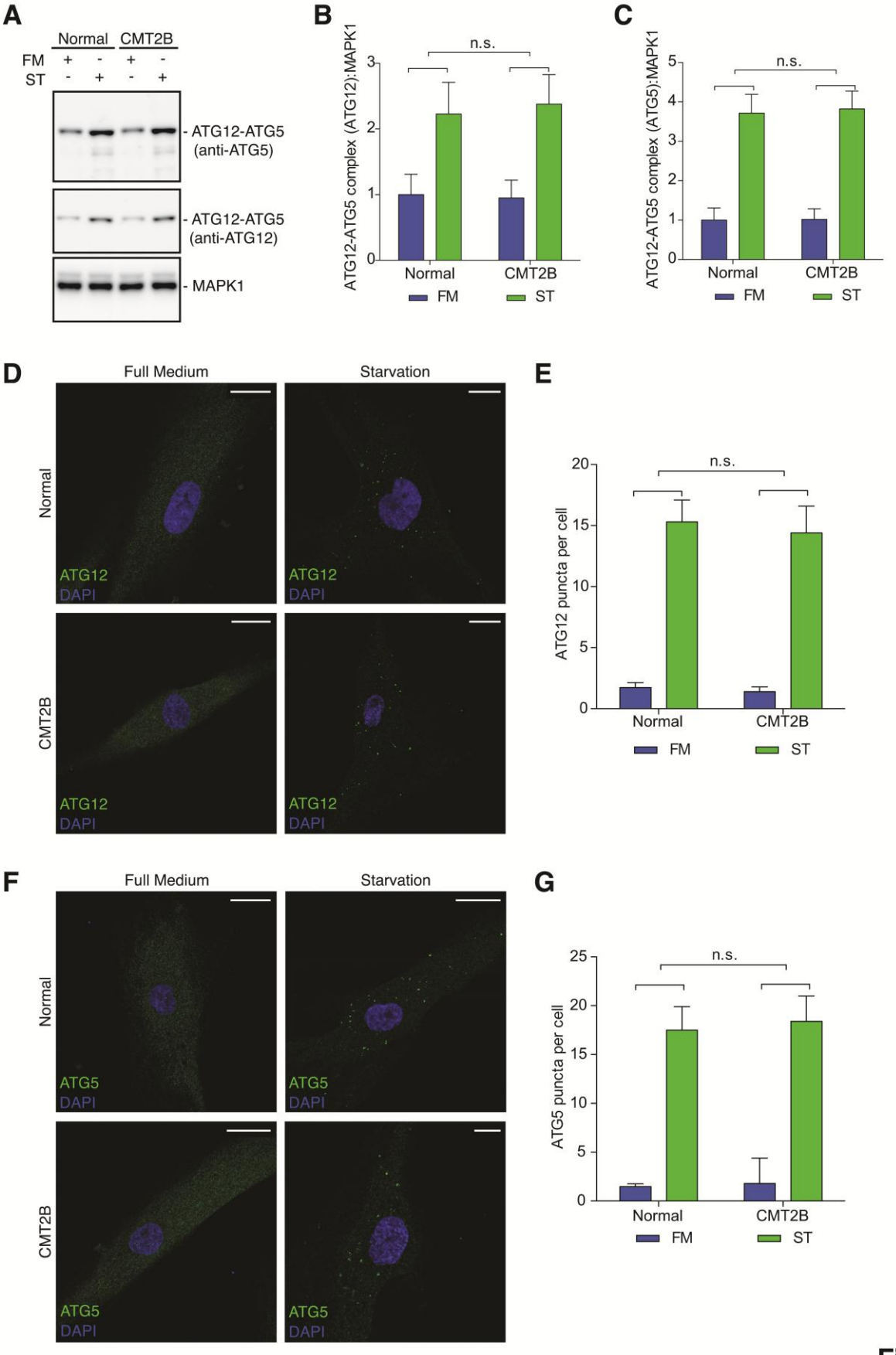

Fig.6